Rotor Performance Predictions of a Next Generation Mars Science Helicopter

Dorsa Shirazi
Aerospace Engineer
NASA Ames Research Center
Moffett Field, CA, USA

Athena Chan
Mechanical Engineer
NASA Ames Research Center
Moffett Field, CA, USA

Wayne Johnson
Aerospace Engineer
NASA Ames Research Center
Moffett Field, CA, USA

ABSTRACT

Since Ingenuity took flight and proved aerial capabilities on Mars, the horizon for rotorcraft on the Red Planet has only expanded. One proposed future Martian rotorcraft is the Mars Science Helicopter (MSH). The MSH is a hexacopter capable of carrying scientific payloads. As a part of its joint development by NASA Ames Research Center (ARC) and the Jet Propulsion Laboratory (JPL), key MSH rotor components will be tested inside the in-development Reduced Atmospheric Pressure Testing Of Rotors (RAPTOR) wind tunnel in the Planetary Aeolian Laboratory (PAL) at NASA ARC. In preparation for the test, the Comprehensive Hierarchical Aeromechanics Rotorcraft Model (CHARM) analysis was utilized to predict the aerodynamic performance for one MSH hexacopter isolated rotor. This paper provides an overview of the planned experiments involving the MSH reference blades, as well as CHARM pretest predictions of rotor performance in hover and forward flight. Additionally, the interference effects of wind tunnel walls on rotor performance will be evaluated to inform the test matrix of the upcoming test in the RAPTOR tunnel.

NOTATION

c	chord length [m]
N	number of blades
R	rotor radius [m]
T	thrust (shaft axis) [N]
C_P	power coefficient
C_Q	torque coefficient
C_T	thrust coefficient (shaft axis)
C_X	drag coefficient (wind axis, + aft)
C_{M_x}	roll moment coefficient (+ toward retreating side)
C_{M_y}	pitch moment coefficient (+ noise up)
V_{tip}	rotor tip velocity [m/s]
V_∞	free stream velocity [m/s]
α	angle of attack [degree]
ρ	air density [kg/m^3]
σ	rotor solidity
Ω	angular velocity [rad/s]
CFD	computational fluid dynamics
CIFER	Comprehensive Identification from FrEquency Response
COTS	commercial off the shelf
CVC	constant vorticity contour
FEA	finite element analysis
FF	forward flight
FM	figure of merit
LMU	load measurement unit
MARSWIT	MARtian Surface WInd Tunnel
MART-I	Mars Aerodynamic Rotor Test-I
MSH	Mars Science Helicopter
PAL	Planetary Aeolian Laboratory
RAPTOR	Reduced Atmospheric Pressure Testing Of Rotors
RC	remote control
RPM	revolutions per minute
SIT	system identification test
SUT	spin up test
VTOL	vertical take-off and landing

INTRODUCTION

The advantages of utilizing rotorcraft in the exploration of Mars include covering greater distances in a shorter time, capturing multiple vantage views from different altitudes, the ability to traverse challenging terrain inaccessible to rovers, and using the vehicle as a utility platform to transport science instruments and other equipment. Additionally, some scientific investigations can only be achieved via low-level flight. However, achieving flight on Mars is a challenge due to the planet's conditions, including extreme temperature changes, low atmospheric density—roughly 1% of Earth's—reduced

speed of sound, and the predominantly carbon dioxide-based atmosphere. The result is a low Reynolds number, compressible flow operating condition. Despite the success of the Ingenuity Mars Helicopter [1], there is so much more to learn about rotorcraft aerodynamics on Mars. To aid in improving the foundational understanding of Mars rotor aerodynamics, both experimental work and computer simulations are underway at NASA Ames Research Center to help usher in the next generation of Martian rotorcraft.

NASA Ames has a long history with the development and advocacy of Mars rotorcraft [2]. As part of this effort, the conceptual design of the Mars Science Helicopter was developed prior to the first flight of Ingenuity [3]. The current hexacopter design weighs an estimated ∼17 kg and is capable of carrying ∼2 kg of scientific payload, Figure 1.

**Figure 1. Mars Science Helicopter conceptual design [3].**

The Comprehensive Hierarchical Aeromechanics Rotorcraft Model (CHARM) [4, 5] analysis was used to predict the aerodynamic performance for single isolated rotor; the estimated thrust, moments, and power are used in the mechanical stress analysis of test stand development. The CHARM results presented in this paper represent the first detailed study of MSH rotor performance to be presented in literature.

There are currently three experimental tests planned for the MSH rotor: 1) Spin Up Test (SUT), 2) Forward Flight Test (MART-I), which will be the first wind tunnel test of MSH forward flight performance, and 3) System Identification Test (SIT), which will explore the relatively novel rotor dynamics of Mars rotors.

The Spin Up Test is primarily a check-out test required to qualify the MSH reference blades for testing in the Reduced Atmospheric Pressure Testing Of Rotors (RAPTOR) tunnel. SUT will spin two blades up to 110% of the planned maximum RPM for in-tunnel testing.

The Mars Aerodynamic Rotor Test-I is a research test with the goal of collecting the first set of wind tunnel data on one MSH rotor's aerodynamic performance. MART-I will spin four blades in the new RAPTOR tunnel. RAPTOR is located inside the Planetary Aeolian Laboratory (PAL) [6], a NASA Ames Research Center facility. This testing mirrors foundational forward flight testing of surrogate rotors tested under Mars-like densities in the MARtian Surface WInd Tunnel (MARSWIT) [7]. MARSWIT has a test section of 1.3 m by 1.3 m, and is also located inside the PAL.

The System Identification Test seeks to validate the MSH rotor's linear dynamics model against measured data. SIT will spin four blades and excite the rotor in five degrees of freedom: heave, lateral/longitudinal translation, and pitch/roll, Figure 2.
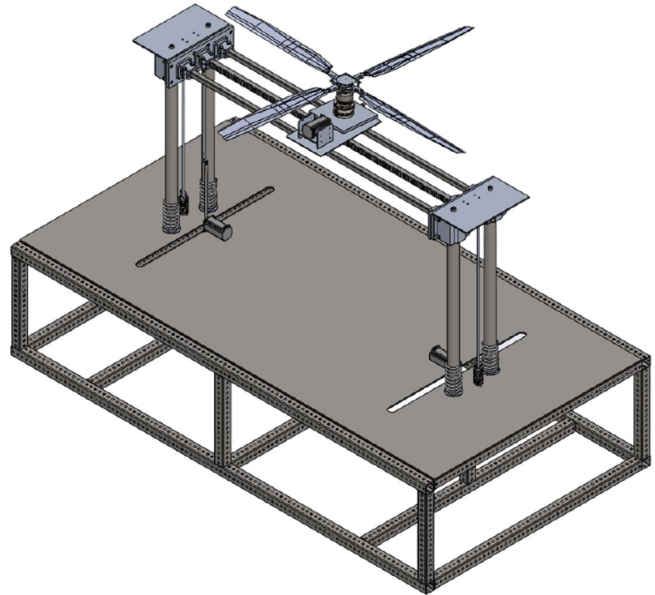
Figure 2. Preliminary design of System Identification Test stand.

The resulting forces and torques will be measured and recorded. The collected data will then be post-processed using Comprehensive Identification from FrEquency Response (CIFER) [8, 9], a system identification software, in order to extract linear stability and control derivatives. SIT will be performed in the PAL at low density atmospheric conditions in conjunction with a wind wall.

This paper will cover the following: 1) New hardware and facilities developed for testing the MSH reference blade, and 2) CHARM simulations to inform the SUT and MART-I test matrix.

MSH REFERENCE BLADE

The MSH rotor has a diameter of 1.374 m and a hub diameter of 0.174 m. The rotor has an optimized linear twist of –18 degrees and cutout at 9% of the rotor radius (0.09R). The rotor has a nonlinear chord length with an average chord of 0.0958 m [3], Table 1. The rotor has a blade thickness of t/c = 8% from the root to 0.22R and t/c = 1% from 0.50R to the tip of the rotor [3]. The blade thickness transitions from t/c = 8% to t/c = 1% between 0.22R and 0.50R.

The MSH reference blade features a very thin airfoil with sharp leading and trailing edges that taper off to a 0.5 mm thickness. Manufacturing the blades proved to be challenging due to its geometry and material, discussed as follows. In 2021, Sensenich successfully manufactured the MSH reference blade. The blade features between 1-3 plies of carbon fiber plies, a spar made of carbon tape, a foam core, and

an aluminum root; with nominal mass of 90 grams, Figure 3. Figure 3 shows the MSH blade and cross section view at r/R=~19%. Note that the radius is defined as the distance from the center of the hub to the tip of the rotor blade.

Table 1. MSH rotor parameters.

Parameters	Values
Radius of blade	0.687 m
Number of blades	2, 4
Average chord	0.0958 m
Linear twist rate	-18 degree/span
Rotor disk area	2.158 m
Solidity ratio	0.0941, 0.1881
Pitch at 75% of the radius	0 degree
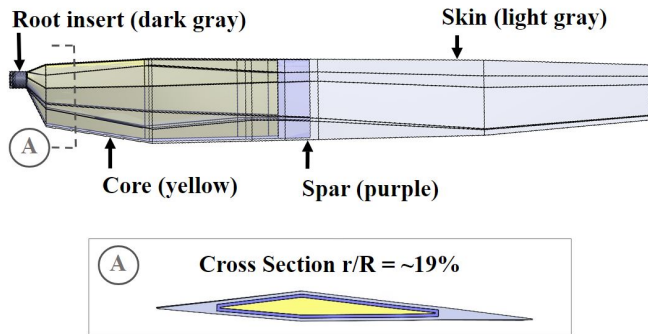
Figure 3. Mars Science Helicopter blade structure and cross-section view at r/R=~19%.

With the manufacturability of the blades proven, a composite structural analysis was then performed on the blades by Sensenich. Thrust and torsional bending loads were obtained via Comprehensive Analytical Model of Rotorcraft Aerodynamics and Dynamics II (CAMRAD II) [10] at NASA Ames Research Center and provided to Sensenich to apply the proper centrifugal tension and bending loads on the layups. The Sensenich analysis showed good confidence that the blades would maintain structural integrity at 3300 RPM, the highest speed the MSH would experience under current test plans. However, the composite structural analysis identified two non-linear points of interest at the blade's 15% and 55% radial station, where the safety factor could not be ascertained analytically, hence the importance of a SUT prior to any other rotor testing.

TEST STANDS

Designing an experimental test stand to operate under Martian conditions with primarily commercial off the shelf (COTS) components proved to be challenging on many fronts. First, the low air density reduces the reliability of convection as a means of thermal dissipation. Second, outgassing and voltage arcing were a concern. Third, the small amount of thrust generated by the rotor blades compared to the weight of the motor, coupled with the high moment generated when the rotor disk is pitched, made finding a suitable six-axis load cell difficult. The large moment required sizing up a load cell, which

then increased the full-scale percent error. For all stands, a minimum safety factor of 3 on yield is required on standard test stand components; exceptions may be made if additional analysis and/or constant monitoring of the part is applicable. Predicted rotor loads from CHARM simulations were used to perform Finite Element Analysis (FEA) on test stand components using SolidWorks simulations.

This section will describe the Spin Up Test stand and Mars Aerodynamic Rotor Test-I stand in greater detail. The System Identification Test stand is still in the preliminary stages of design and therefore not discussed.

Spin Up Test Stand

Centrifugal loading is the dominant structural stressor on the MSH reference blade, as the generated aerodynamic loads are comparatively small due to the low-density operating condition inside the PAL. Thus, the primary purpose of the Spin Up Test stand, see Figure 4, is to spin two MSH reference blades up to a minimum of 110% (~2500 RPM) of the highest speed planned during MART-I (~2100 RPM) behind the safety of blast shields inside the PAL test chamber to experimentally confirm the blades can handle the operational centrifugal loading. Another check-out run on the SUT will be executed at ~3300 RPM to qualify the blades for the SIT, which anticipates a maximum RPM of ~3000. The structural analysis of this test stand was conducted at 3300 RPM, representing the worst-case scenario.

Figure 4. Spin Up Test stand.

Another purpose of the SUT is to validate the motor can performance at reduced pressure under load. During SUT runs, blades will be set to 0 degree collective and be spun at the PAL in reduced pressure. A small amount of thrust will still

be generated despite the 0 degree collective due to the linear twist of the blades.

The SUT uses a blend of COTS and custom components to enable rapid design of the stand while minimizing costs. A COTS force-torque sensor, also known as a Load Measurement Unit (LMU), from a large propellor drone test stand is used to measure torque and thrust. The LMU is used in conjunction with the COTS data acquisition system. The rotorhead has a manually adjustable feature that allows for fine tuning of the blade pitch; no swashplate or servos are used with the SUT in effort to keep the design simple. The motor is oversized by 100% of the SIT's torque requirement at the maximum RPM. The intent is to use the same motor for the SUT, MART-I, and SIT. Since the SIT will be the most demanding, the motor was sized to its requirements. Also, high-impact resistant shields from Total Shield will be used to protect property and personnel in the event of a blade loss.

Mars Aerodynamic Rotor Test-I Stand

The MART-I stand operates with a 4-bladed rotor, representing one of the six rotors in the MSH conceptual design. The primary goal of the MART-I is to collect data on the MSH blades at an advance ratio of 0.18. This advance ratio is consistent with the maximum design target flight speed of the MSH and its nominal rotor RPMs. The advance ratio is defined as Equation 1, where V_∞ is the free stream velocity, or the tunnel speed, V_{tip} is the rotor tip speed, α is the angle of attack, and μ is the advance ratio. The planned tunnel speed is 28 m/s. This is approximately the design forward flight speed for the MSH conceptual vehicle. Furthermore, 28 m/s represents a major speed increase—and design challenge—for not only Mars rotorcraft, but also for Mars rotorcraft wind tunnel testing. Ingenuity's maximum speed is ∼10 m/s, and to date, Mars rotorcraft wind tunnel testing has been limited to ∼10 m/s.

$$\mu = \frac{V_\infty cos(\alpha)}{V_{tip}} \quad (1)$$
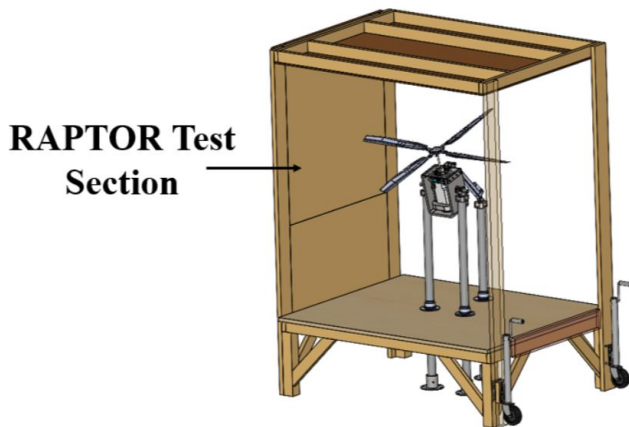
Figure 5. Preliminary Mars Aerodynamic Rotor Test-I stand design, inside RAPTOR test section.

For MART-I, the blades also feature collective control up to 16 degrees; the rotor shaft angle can also pitch up to 15 degrees into the wind and 15 degrees away from the wind. Figure 5 shows the test stand with 4-bladed rotor at a negative pitch angle inside of the RAPTOR test section.

The MART-I stand uses a 3-strut design. A modified COTS Remote Control (RC) rotorhead is used, with the blade grips swapped out for custom grips that can interface with the MSH blades. RC servos offer collective and cyclic control, though current test plans will only utilize the collective. The motor is directly connected to the rotor shaft. The motor sits atop a six-axis load cell, which will measure moments and forces in all three axes. Also, a linear actuator will pitch the rotor disk about a pair of pivot pins.

PLANETARY AEOLIAN LABORATORY

The SUT, MART-I, and SIT will take place in the PAL's test chamber, Figure 6. The desired pressure is 7-15 mbar to simulate flight conditions on Mars.

Figure 6. PAL; low pressure test chamber is contained within the tall rectangular tower.

The temperature in the PAL test chamber is monitored but not actively controlled. The PAL has a height of 30 m and a volume of 4000 m³, so temperature changes in the test environment are expected to be minimal. There are currently no plans to backfill the test chamber with any specific gas blends.

The PAL can be pumped down to 5 mBar for extended durations. The first-ever documented hover test of a rotor under Mars-like densities was conducted in the PAL during 2001-2002 [11]. MARSWIT was used to test a 40-inch diameter surrogate rotor under Mars-like conditions, marking a first of such edgewise testing for Mars rotorcraft research in 2018 [7]. The proposed MSH testing will continue the nearly twenty-five year legacy of Mars rotorcraft research in the PAL.

RAPTOR TUNNEL

The RAPTOR tunnel is a modular wind tunnel currently under construction at NASA Ames to support next-generation Mars rotorcraft testing under forward flight conditions. The baseline tunnel drive system is an electric-motor fan drive, Figure 7. Future plans include the possibility of an air-injection

drive system, which would offer more robust performance at reduced pressures.
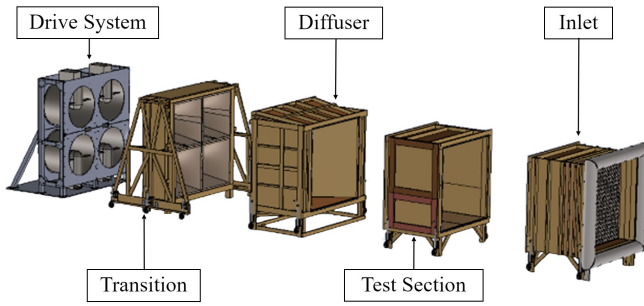
Figure 7. RAPTOR with the fan drive system.

The test section of RAPTOR has a cross sectional area of 2.032 m x 2.032 m, and a length of 1.524 m, Figure 7. The test section is planned to have a wind velocity of 27 m/s. The tunnel's modular design allows test sections to be added or swapped out. The tunnel will be equipped with differential pressure transducers for velocity measurements.

Once RAPTOR construction is completed, the tunnel will be moved into the PAL's test chamber as a much larger alternate to MARSWIT.

CHARM MODEL DESCRIPTION

Computational Fluid Dynamics (CFD) predictions of the MSH reference blades utilizing CHARM have also been underway. CHARM is a comprehensive Vertical Take-Off and Landing (VTOL) aircraft tool developed by Continuum Dynamics Inc (CDI) [4, 5]. The aircraft aerodynamic and dynamic interactions are modeled by combining the fast vortex and fast panel solution [5, 12], which then outputs information such as load, trim, wake geometry, and surface pressure. CHARM simulates real-time, free-wake instability in addition to computing performance of multiple rotors and interaction between the body and rotor wake. The program uses Constant Vorticity Contour (CVC) to model wakes [13] while providing accurate aerodynamic interaction and can produce results in a short computational time.

In the fast panel method, each panel has a constant source and doublet strength, in which the source strengths satisfy the Dirichlet boundary conditions for the ambient flow field. CHARM uses Fast Vortex/Fast Panel methods to characterize the rotor aerodynamic behavior, including the rotor/wake interaction and wind tunnel wall effects, where the wind tunnel is modeled using inviscid incompressible flow. The Fast Vortex and Fast Panel method uses a grouping plan in addition to a validated multi-pole approximation to decrease the computational time by over two orders of magnitude for 10^5 panels. In the grouping technique, the vertices and panels are grouped into nested cells. For the high-density area, these grids will be more refined for nested cells [5, 13].The solution is calculated through multipole expansion and Taylor series extrapolations. The CHARM software is capable of modeling VTOL aircraft aerodynamics in maneuvering and steady

flight conditions, which makes this software an ideal choice for this study.

For this project, CHARM was utilized to predict the pretest performance of the MSH rotor using the reference blade airfoil tables at MART-I/SUT test conditions. This will be the first application of CHARM in the analysis of Mars rotorcraft. CHARM predictions of rotor thrust, power, hover Figure of Merit (FM), C_T, and C_P, are among the outputs of the software tool. As a part of this overall MSH development effort, the rotor aerodynamic loads taken from CHARM have been used as input for stress analysis for the MSH test stand structure and mechanical components. CHARM aero performance simulations have been run for both the 2-bladed SUT rotor geometry and the 4-bladed MART-I rotor geometry without the presence of the test stand. Since SUT will not be conducted inside a wind tunnel, the isolated rotor was simulated in hover without the presence of the RAPTOR section walls. The boundary conditions of the MART-I simulation were matched to the RAPTOR tunnel dimensions.

Comparing CHARM to Other Analysis Tools in Martian Condition

This work is focused on introducing the forward flight test for the MSH rotor and the results of CHARM MSH performance predictions. In order to better understand how CHARM pretest predictions serve as a benchmark for MSH rotor performance predictions, comparing CHARM predictions to other known data sets is prudent. Reference 14 details the comparison between data collected from the Ingenuity prototype experiment in the Jet Propulsion Laboratory 25-ft Space Simulator (JPL SS), CAMRAD II, and RotCFD predictions for Ingenuity's two counter-rotating 2-bladed rotors with a diameter of 1.21 m and at RPM=2600 RPM with a tip speed of 165 m/s.
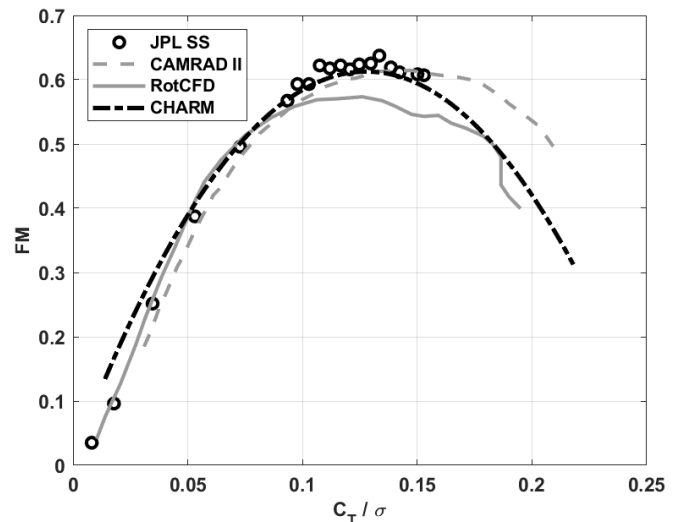
Figure 8. FM vs. C_T/σ - in JPL SS conditions.

The Ingenuity rotors at JPL SS conditions were modeled in CHARM. Figure 8 illustrates CHARM simulation prediction for FM versus C_T/σ for Ingenuity rotors against the

experimental data (JPL SS), CAMRAD II, and RotCFD results from Reference 14. These results indicate that CHARM slightly overpredicts the FM for low C_T/σ, but still provides a good/well-matched prediction for JPL SS experimental data.

SIMULATION RESULTS

CHARM was utilized for pretest flight predictions for the Mars Science Helicopter rotor. For this study, the test variables in Table 2 and Table 3 for 2-bladed and 4-bladed rotors were simulated in CHARM for wind tunnel and free field conditions at different pitch and collective angles, as well as different wind tunnel speeds and rotor RPM.

Table 2. CHARM simulation variables for SUT using 2-bladed rotor.

Variables	Attributes
Number of blades	2
Collective [Deg]	0, 5, 7, 9, 11, 13, 15, 17, 19
Rotor speed [RPM]	1000, 1200, 1400, 1540, 1600, 1800, 1900, 2100, 3000, 3300

Table 3. CHARM simulation variables for SUT using 4-bladed rotor.

Variables	Attributes
Number of blades	4
Pitch angle [Deg,+aft tilt]	0, -6, -12
Collective [Deg]	0, 5, 7, 9, 11, 13, 15, 17, 19
Tunnel speed [m/s]	0, 10, 18, 30
Rotor speed [RPM]	1000, 1900, 2100, 3300
M_{tip}	0.212, 0.402, 0.444, 0.698

Martian conditions were simulated with air density of 0.02 kg/m^3 and kinematic viscosity of 0.001 m^2/s. Since the PAL facility will not be filled in with CO_2 gas, the speed of sound of 340.12 m/s was used. This study aimed to look at different flight conditions to predict the wall effect and determine any limitations the current test matrix might encounter. The airfoil table utilized in the simulation was generated using OVERFLOW by Koning et al. [15]. The airfoil table encompassed a moderate angle of attack range between -10 to 20 degrees for the Reynolds-Mach ratio pairing shown in Table 4.

Table 4. The ratio of Reynolds and Mach numbers of six main airfoil stations used to generate the airfoil table.

Station #	r/R	Re/M	Chord [m]
Station 1	0.0908	11426	0.082
Station 2	0.2500	31214	0.113
Station 3	0.5000	38151	0.108
Station 4	0.7500	29847	0.104
Station 5	0.9000	22024	0.089
Station 6	1.0000	17240	0.079

The MSH airfoil table was patched with the NACA 0012 airfoil table for the missing angle of attacks between $-180 \leq \alpha \leq 180$, which is critical for high advance ratio edgewise forward flight rotor performance prediction [15, 16]. The MSH airfoil table was generated for Martian conditions (CO_2) and used for the pretest predictions of performance in PAL. However, the PAL's test environment has a few discrepancies from actual flight conditions on Mars, namely, the working gas is air (O_2, N_2), and the test chamber temperature will not be actively controlled. This operating condition discrepancy is assumed to present only a small error. In the future, airfoil tables for PAL atmosphere will be generated and used for simulations.

Hover

First, an isolated single, 2-bladed rotor was simulated in hover for C_T/σ from 0.018 to 0.206. A 4-bladed rotor was also simulated for C_T/σ 0.030 to 0.175 at RPM 1000, 1200, 1400, 1540, 1600, 1800, 1900, 2100, 3000, and 3300 (M_{tip} = 0.21 to 0.68). Figure 9 shows the wakes of the isolated 4-bladed MSH rotor in free field at hover and RPM=2100.
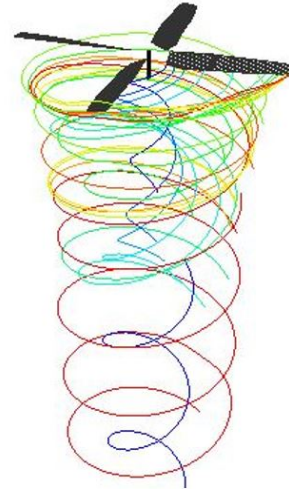
Figure 9. CHARM visualization simulation of the isolated 4-bladed MSH rotor out of ground effect in free field at hover.

The figure of merit vs. C_T/σ are shown in Figures 10-13. The FM values were in the expected range of 0.5 to 0.7 for 2-bladed and 4-bladed rotors. The CHARM results have provided several key insights regarding the performance of the MSH reference blade. Figures 10 and 12 show there is a decrease in FM once C_T/σ surpasses approximately 0.13; the 4-bladed rotor also reaches a higher FM of approximately 0.63. Figure 11 expands the peak FM region of Figure 10. These results indicate that a 2-bladed rotor at C_T/σ of 0.13 and RPM 2000 can reach an FM of 0.57, and at C_T/σ=0.12 and RPM 3300 can reach FM of 0.62. This range of FM values is consistent with past observed values for other rotors conducted under Mars atmospheric density conditions. The C_T/σ of the maximum FM and the drop-off/roll-off of figure of merit indicates the beginning of rotor stall. The airfoil drag and, therefore, rotor power significantly increases because over the span of the rotor blades, localized angles of attack have been exceeded, and the local blade section has entered airfoil stall.
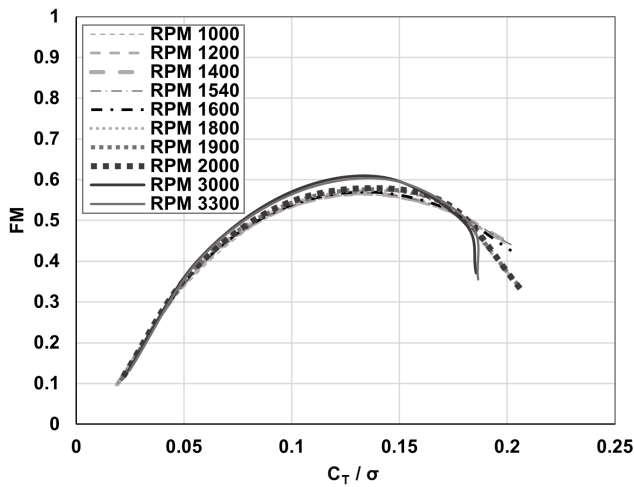
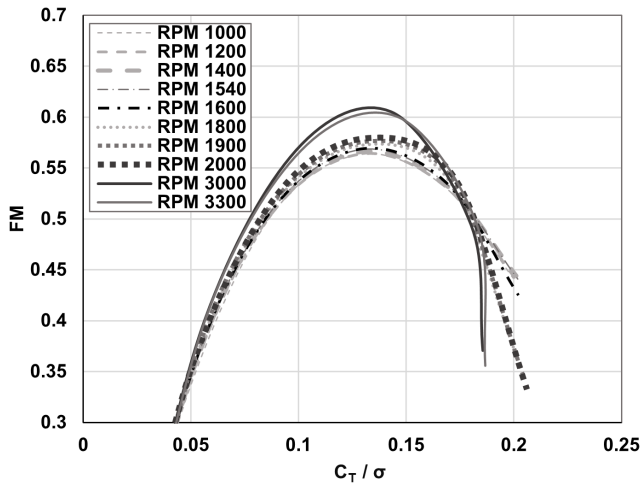**Figure 10. Single isolated 2-bladed MSH rotor in hover – Figure of Merit vs C_T/σ.**

Figure 11. Single isolated 2-bladed MSH rotor in hover – FM vs C_T/σ - focuses on the FM peak.
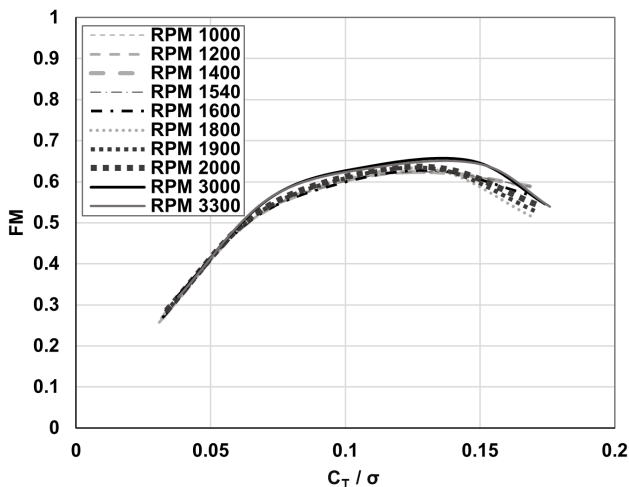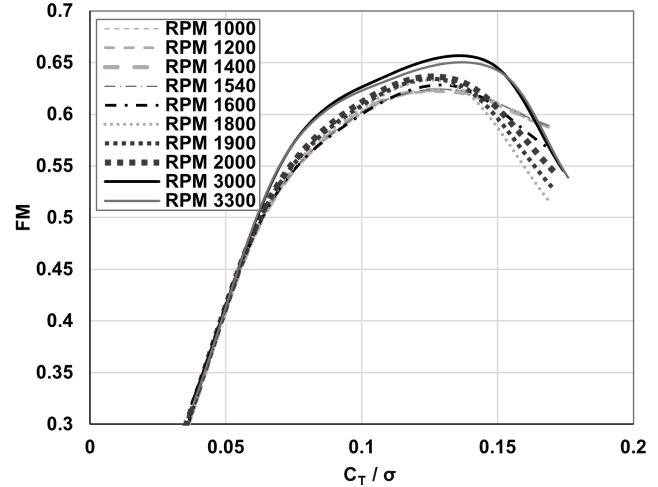

Figure 12. Single isolated 4-bladed MSH rotor in hover – Figure of Merit vs C_T/σ.

The nominal C_T/σ by which rotor stall begins can vary as a function of airfoil choices used, blade twist employed, and rotor disk loading target used in the rotor design. All of these choices also influence how quickly the FM curve drops off once rotor stall has been entered. Comparison of Figures 10 and 12 reveal the 4-bladed rotor has a slightly better figure of merit than the two-bladed rotor. This is well-known behavior in rotorcraft research.

Figure 13. Single isolated 4-bladed MSH in hover – FM vs C_T/σ – focuses on the FM peak.
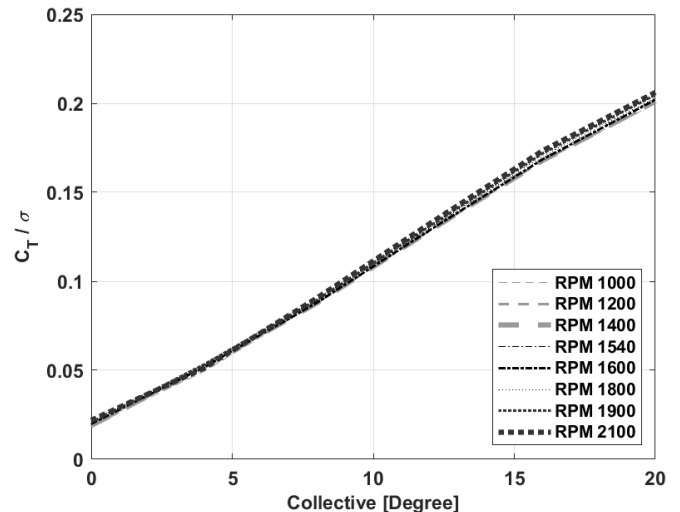
Figure 14. Single isolated 2-bladed MSH rotor in hover – C_T/σ vs collective.

The hover study is focused on a 2-bladed rotor, Figure 14-16, since that is the configuration tested in the SUT first. Additional hover results and plots for the 4-bladed rotor can be found in Appendix A.

The plan is to test up to a collective of 16 degrees in the MART-I; this plan may change, however, as more information from simulation and testing is acquired.

Additionally, the hover performance of the 2-bladed MSH rotor with fixed collective at 3300 RPM, at pitch angles of 0, 6, and 12 degrees, was simulated to support the required checkout system. The result shows that at C_T/σ of 0.13 , an FM of

7

0.62 can be reached at 3300 RPM. Note that the solidity for the 2-bladed rotor is approximately 0.0941, and the 4-bladed rotor is approximately 0.188. Figure 16 predicts a significant influence from Re_{tip} and, to a lesser degree, M_{tip} on rotor performance, especially with respect to rotor power and airfoil profile drag.
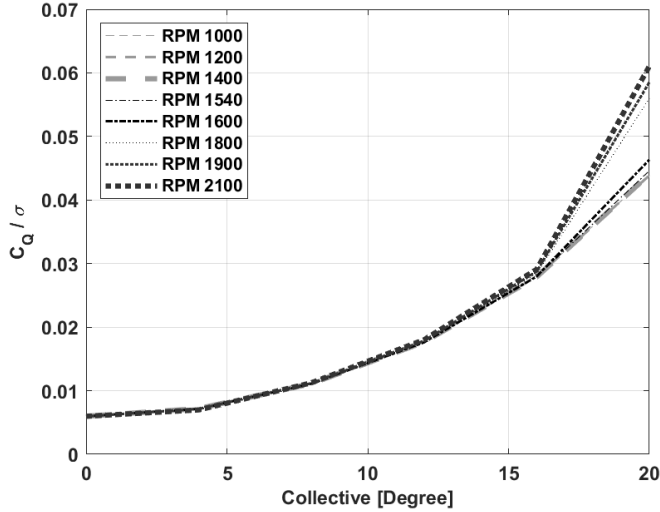
Figure 15. Single isolated 2-bladed MSH rotor in hover – C_Q/σ vs collective.
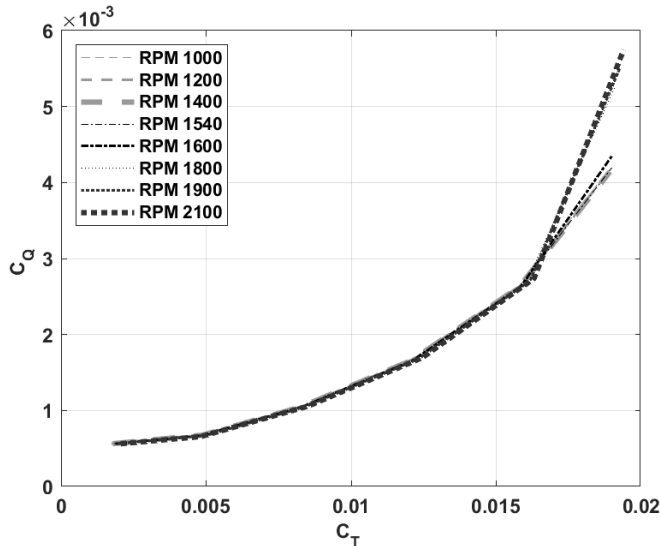
Figure 16. Single isolated 2-bladed MSH rotor in hover – C_Q vs C_T.

Forward Flight

For CHARM forward flight cases, the RAPTOR test section dimension was modeled as a 2.032 m by 2.032 m cross-section and length of 20 meters to allow the flow to develop fully. The MSH test stand was not included in CHARM simulations. Based on the hover pretest prediction for the 4-bladed rotors presented in Figure 12-13, the highest C_T/σ value that can be attained at 2100 RPM is 0.13. To determine the wind tunnel velocity, a single 4-bladed MSH rotor was simulated

within the modeled test section at 2100 RPM while being trimmed to a C_T value of 0.024 for 0, -6, -12, and -16 pitch angles while sweeping the tunnel velocity from 10, 15, 20, 25, to 30 m/s. The relationship between the advance ratio and wind tunnel velocity experienced at each pitch angle is illustrated in Figure 17 for RPM 2100 and 1200. As mentioned at the beginning of this paper, the primary objective of the MART-I is to gather data on the MSH blades at an advance ratio of 0.18, which would require a tunnel velocity of approximately 28 m/s. However, given the current RAPTOR tunnel fan-based drive system, this velocity cannot be achieved, and as such, the focus of this paper will be for velocities of 10 and 18 m/s. Pretest predictions for velocity of 30 m/s can be found in Appendix C.

Rotor performance in forward flight was predicted for tunnel speeds of 10 and 18 m/s at RPM 1000, 1900, and 2100 with fixed collective at 5, 7, 9, 11, 13, 15, 17, 19 degrees and pitch angles of 0, -6, and -12 degrees. The current design of the MSH rotor includes collective control for vehicle trim. Table 5 presents the advance ratio of the single 4-bladed MSH rotor at different RPMs and tunnel speeds.

Table 5. Advanced ratio of the single 4-bladed MSH rotor at different tunnel speed and RPMs.

	Tunnel Speed [m/s]		
RPM	10	18	30
1000	0.139	0.250	0.417
1900	0.073	0.132	0.219
2100	0.066	0.119	0.199
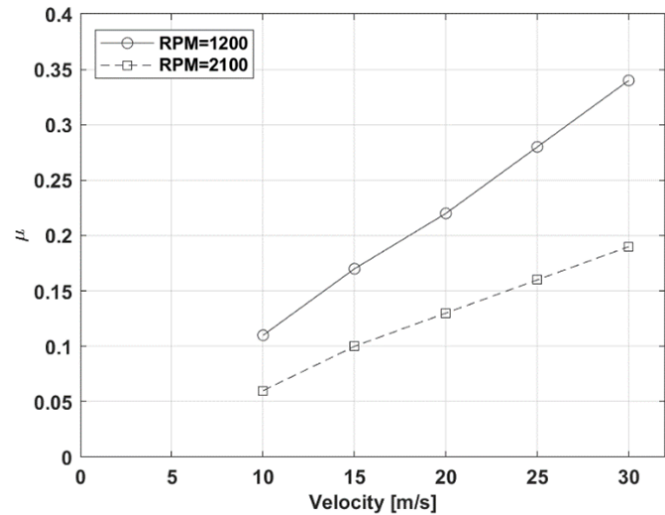
Figure 17. CHARM prediction: advance ratio vs. velocity for isolated 4-bladed MSH rotor in RAPTOR tunnel at RPM 1200 and 2100.

Figures 18 and 19 show the simulation results of C_T and C_P vs. collective at 1000 RPM for different tunnel speeds and pitch angles. Each data point shown is an average over 100 rotor revolutions.

Figure 18 indicates that at a tunnel speed of 10 m/s and a pitch angle of 0 degrees, the same amount of thrust can be achieved

at a speed of 18 m/s and a pitch angle of -6 degree. However, slightly more power will be required at 18 m/s, as suggested in Figure 19. Predictions of the parasite power coefficient and drag coefficient versus collective are shown in Figures 20 and 21, respectively, for RPM 1000.

Figure 20 shows that at higher tunnel speeds, the parasite power coefficient is more sensitive to the change in shaft and collective angles. These results suggest that lower drag can be experienced at collective of 5 degrees, and a pitch angle of -6 degrees; thus, -6 degrees pitch might be a better condition to increase or decrease the wind tunnel speed compared to pitch angles of -12 degrees when drag is higher.
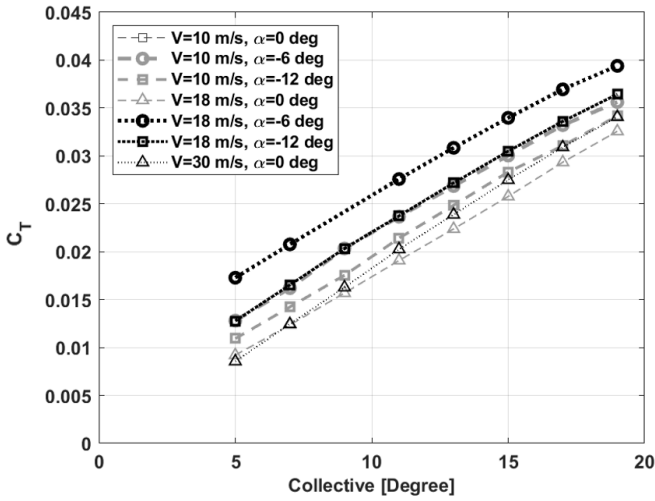
Figure 18. Predicted C_T vs. collective for isolated 4-bladed MSH rotor in RAPTOR tunnel at RPM=1000.
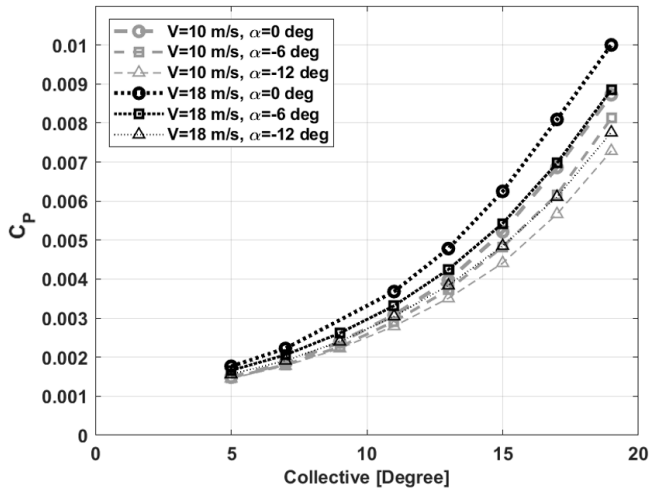
Figure 19. Predicted C_P vs collective for isolated 4-bladed MSH rotor in RAPTOR tunnel at RPM=1000.

Figures 22 and 23 show the computational results of roll moment (C_{M_x}) and pitch moment (C_{M_y}) versus collective for tunnel speeds of 10 and 18 m/s and pitch angles of 0, -6, and -12 degrees. As expected, when the collective increases, the roll moment coefficient grows as well. These results show that C_{M_x} is more sensitive to a changes in tunnel speeds at all three pitch angles compared to the C_{M_y}.

Also, Figure 23 shows for collective <7 degrees, the pitch moment coefficient is slightly higher at lower tunnel speed, but for collective >9 degrees, the pitch moment coefficient is higher for faster tunnel speed. Additional forward flight results for RPM=1000 for the 4-bladed rotor is found in Appendix B.
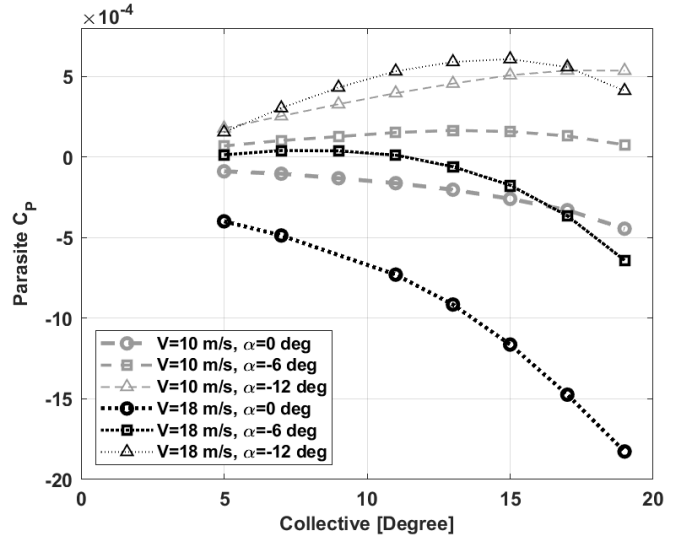
Figure 20. Predicted parasite power coefficient vs. collective for isolated 4-bladed MSH rotor in RAPTOR tunnel at RPM=1000.
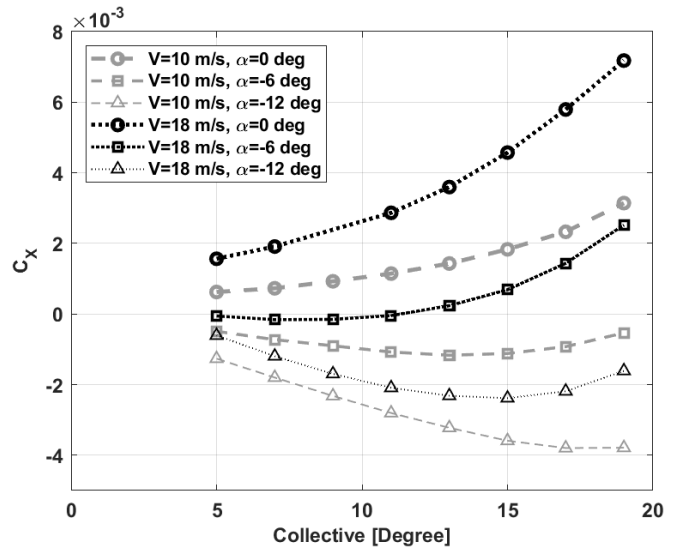
Figure 21. Predicted drag coefficient vs. collective prediction for single 4-bladed MSH rotor in forward flight in RAPTOR tunnel at RPM=1000.

Similar predictions were performed for the 4-bladed rotor at forward flight speeds of 10 and 18 m/s, RPM of 1900, fixed collectives of 5, 7, 9, 11, 13, 15, 17, 19 degrees, and pitch angles of 0, -6, and -12 degrees. Results are shown on Figure 24-29. Figure 24 shows C_T versus collective. Increasing the RPM resulted in a decrease in produced thrust. The similarity in the slope between Figures 18 and 24 indicates the sensitivity to collective has not been changed by increasing the RPM from 1000 to 1900.

9
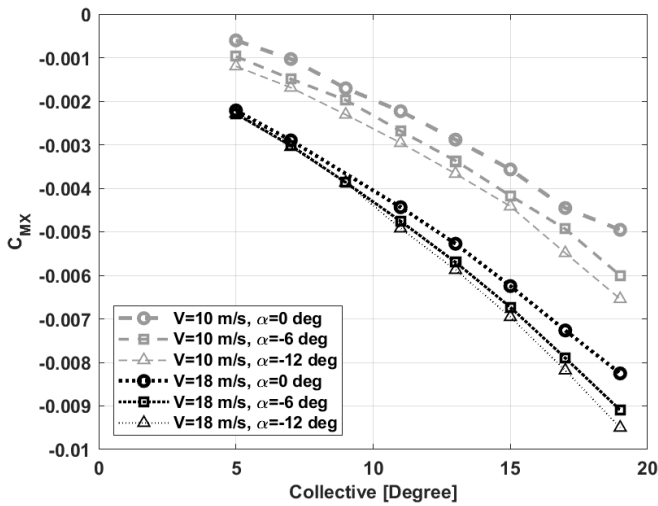
Figure 22. Predicted roll moment coefficient. vs. collective for a single 4-bladed MSH rotor in RAPTOR tunnel at RPM=1000.
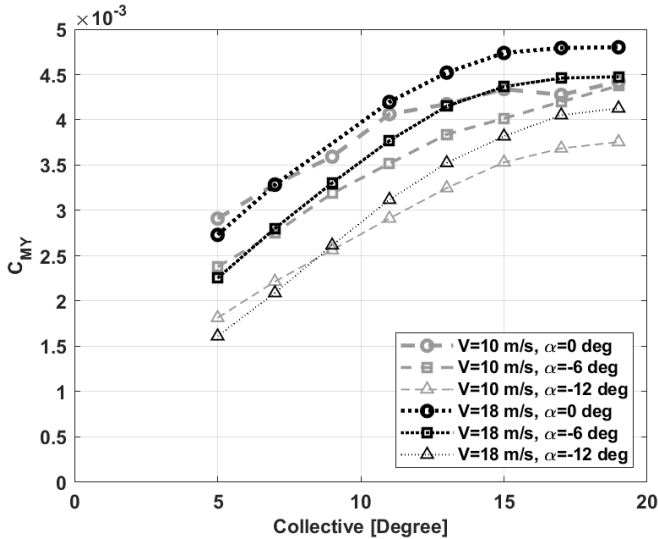
Figure 23. Predicted pitch moment coefficient vs. collective for a single 4-bladed MSH rotor in RAPTOR tunnel at RPM=1000.
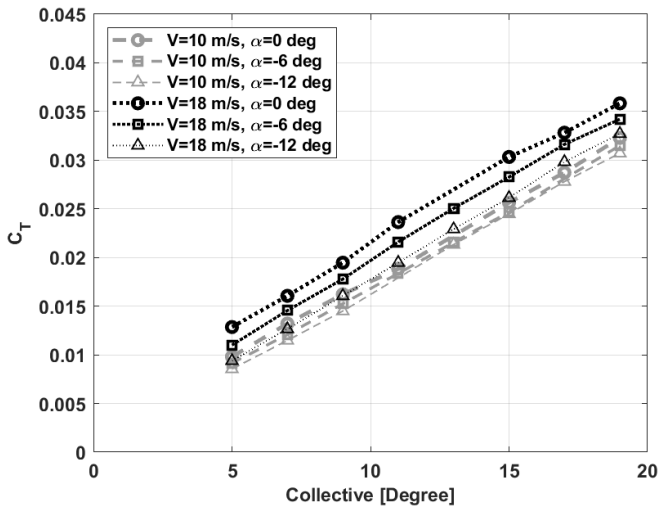

Figure 24. Predicted C_T vs. collective for a single 4-bladed MSH rotor in RAPTOR tunnel at RPM=1900.
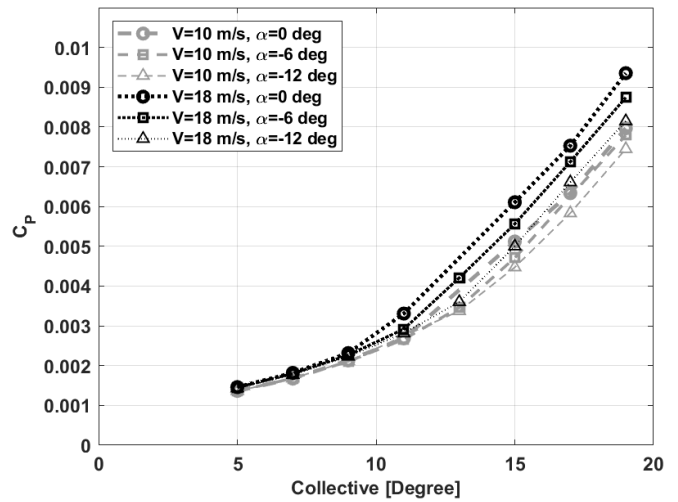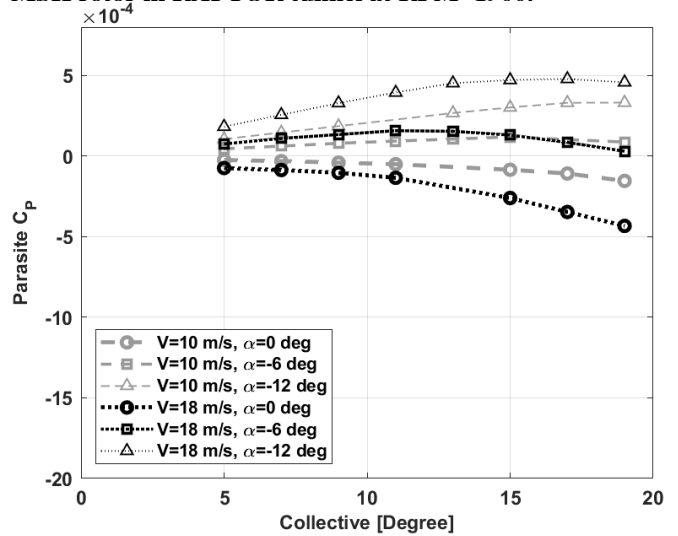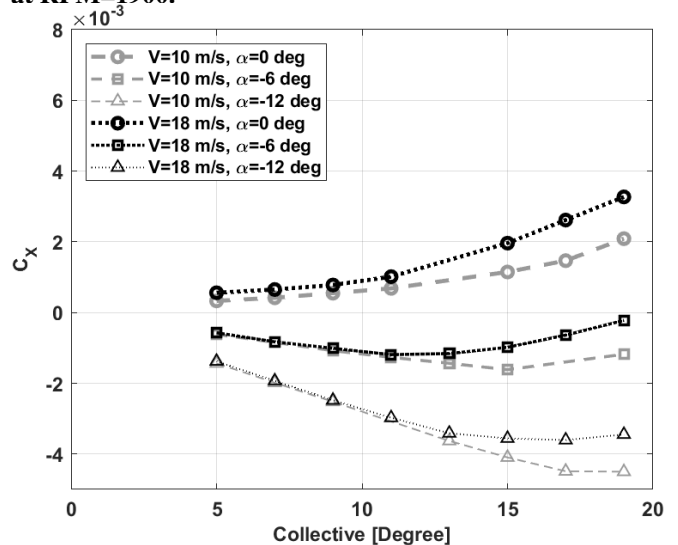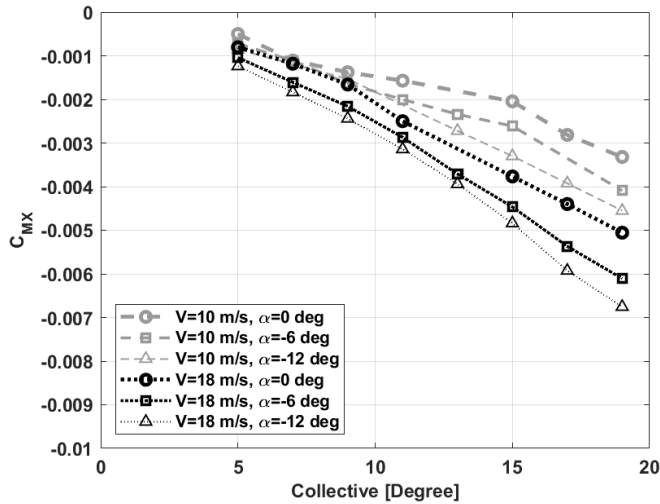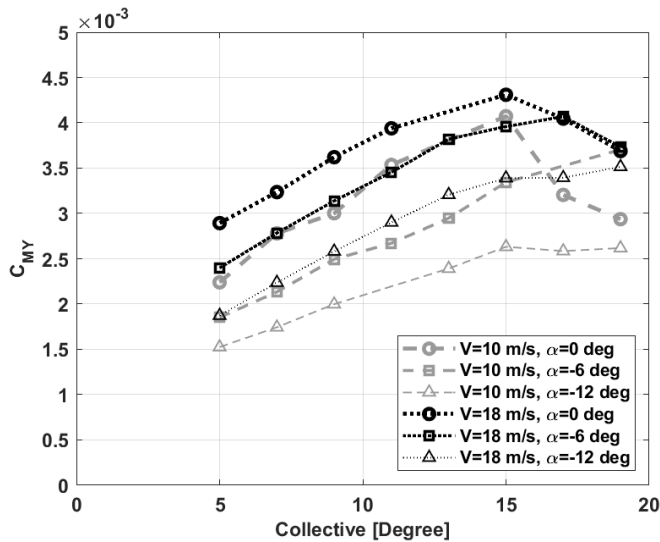

Figure 25. Predicted C_P vs. collective for a single 4-bladed MSH rotor in RAPTOR tunnel at RPM=1900.

Figure 26. Predicted parasite power coefficient vs. collective for a single 4-bladed MSH rotor in RAPTOR tunnel at RPM=1900.

Figure 27. Predicted drag coefficient vs. collective for a single 4-bladed MSH rotor in RAPTOR tunnel at RPM=1900.

10

The results of Figures 19 and 25 show that at RPM 1900 (Figure 25) at the same pitch and collective angle, a higher thrust will be produced at a lower power required compared to RPM 1000. Figure 26 shows the parasite power coefficient for RPM=1900 at the lower tunnel speed of 10 m/s decreased compared to RPM 1000 results. Figure 26 shows the parasite power coefficient for RPM 1900 at tunnel speed of 10 m/s decreased compared to RPM=1000 results.

Figure 28. Predicted roll moment coefficient vs. collective for a single 4-bladed MSH rotor in RAPTOR tunnel at RPM=1900.

Figure 29. Predicted pitch moment coefficient vs. collective for a single 4-bladed MSH rotor in RAPTOR tunnel at RPM=1900.

Figure 27 suggests that at RPM=1900 and pitch angle of -6 and -12 degrees at both tunnel speeds, the drag coefficient sensitivity to change in collective angle is minimal from a collective of 5 to 12 degrees. As the pitch angle increases, the angle of the incident increases therefore, the drag increases as well, and these effects are more pronounced in the higher tunnel speed.

Figure 28 shows a slower decrease in roll moment coefficient for pitch angles of 0, -6, -12, for both tunnel speeds compared to RPM=1000, Figure 22. Figure 29 shows the pitch moment coefficient became more sensitive to an increase in tunnel speed at RPM 1900. This result indicates the possibility of the stronger wall effects occurring at tunnel speeds of 10 m/s at RPM 1900; therefore, additional simulation is required at free field.
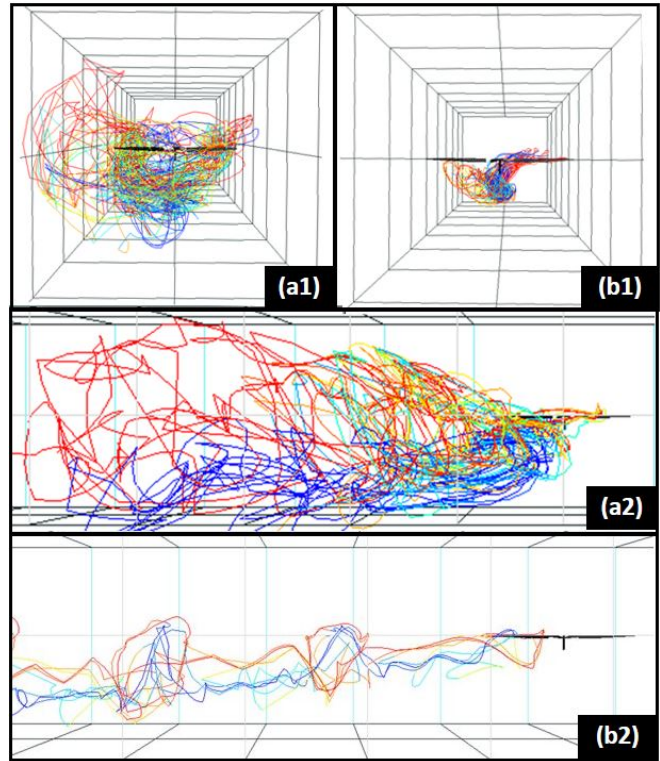
Figure 30. A single 4-bladed MSH rotor in RAPTOR at RPM=1900, pitch angle of 0 deg, collective of 9 deg, and speed of 10 m/s (a1, a2), and 30 m/s (b1, b2) - show front view (a1,b1) and side view (a2,b2).

To better study the wall effect on the MSH isolated rotor results, the rotor wake was visualized inside of the wind tunnel for RPM of 1900 at a pitch angle of 0 degree, collective of 9 degree, and for tunnel speeds of 10 and 30 m/s, respectively.

Figure 30 shows flow visualizations of a single 4-bladed MSH rotor inside of the RAPTOR test section. Figure 30 (a1, b1) shows the front view of the rotor and rotor wake interaction with the wind tunnel wall, and Figure 30 (a2, b2) shows the side view for tunnel speed of 10 m/s (a1, a2) and 30 m/s (b1, b2). This visualization confirms the wall effect at the lower tunnel speed of 10 m/s whereas at the higher tunnel speed, the wake is convected without interacting with the walls downstream.

To study the wall effect further, the simulations were reformed with and without the wind tunnel walls and for a collective sweep at RPM=1900 and tunnel speed=10 m/s.

The difference between the wind tunnel and free field results in Figures 31-33 suggests a significant influence of wall effects on the MSH rotor under the tunnel operating conditions

of interest. This implies that in all future correlation work be-tween rotorcraft analysis software and the experimental mea-surements, the tunnel walls will need to be modeled to ac-curately compare the experiment to the analysis. The same simulation cases were run for RPM 2100 for a 4-bladed MSH rotor in the RAPTOR tunnel at forward flight speeds of 10 and 18 m/s, collective of 5, 7, 9, 11, 13, 15, 17, 19 degrees, and a pitch angle of 0, -6, and -12 degree.
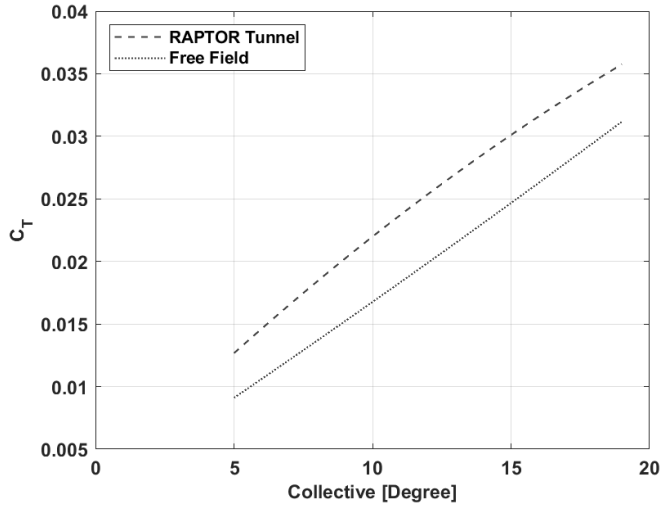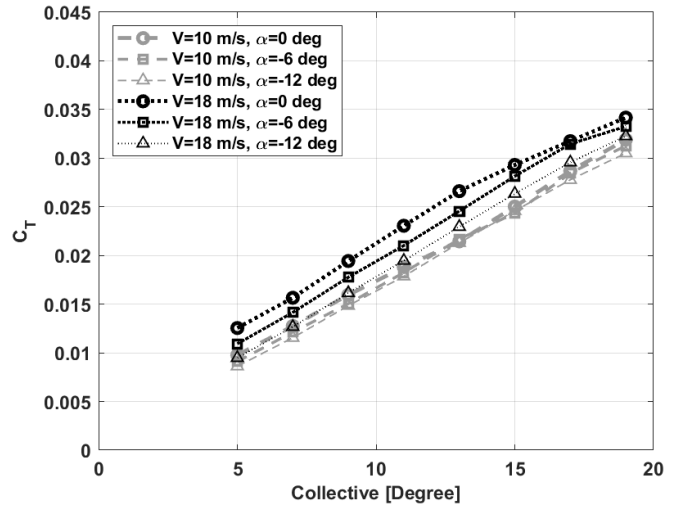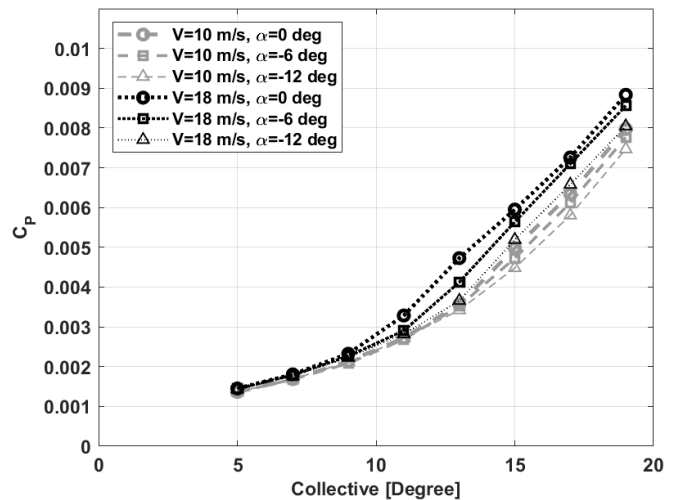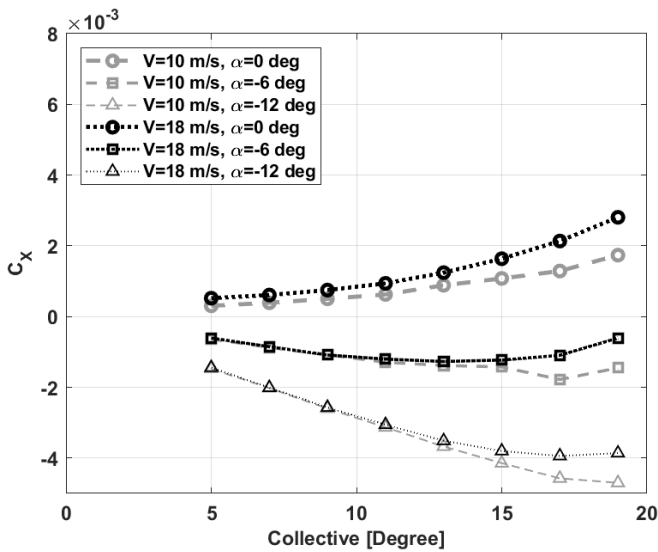

Figure 31. Predicted C_T vs. collective for a single 4-bladed MSH rotor at RPM=1900, forward speed=10 m/s, and pitch angle =0 deg in free field and in the RAPTOR tunnel.
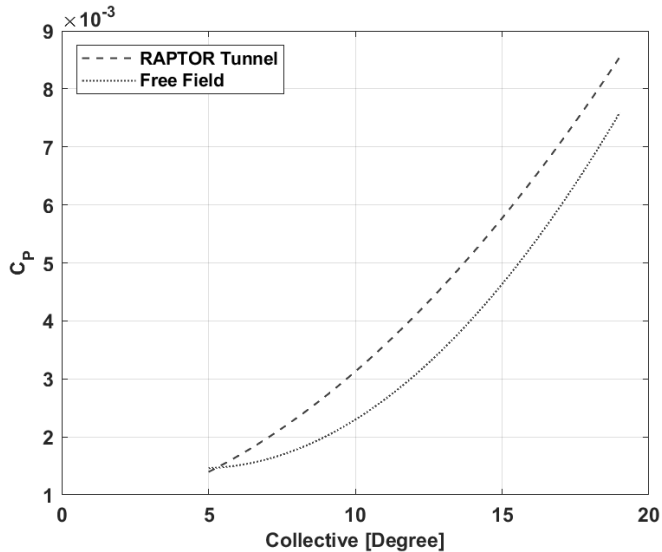
Figure 32. Predicted C_P vs. collective for a single 4-bladed MSH rotor at RPM=1900, forward speed=10 m/s, and pitch angle =0 deg in free field and in the RAPTOR tunnel.

The thrust and power coefficient results vs. collective angle for RPM=2100 have very similar results to RPM=1900, with Figures 25-36, indicating that an increase in RPM did not in-crease the thrust or affect the power significantly. The parasite power coefficient, pitch, and roll moment coefficient vs. col-lective results can be found in Appendix B. Figure 36 shows that the drag coefficient is less sensitive to change of collec-tive between 5 to 13 degrees for tunnel speeds of 10 and 18 degrees.
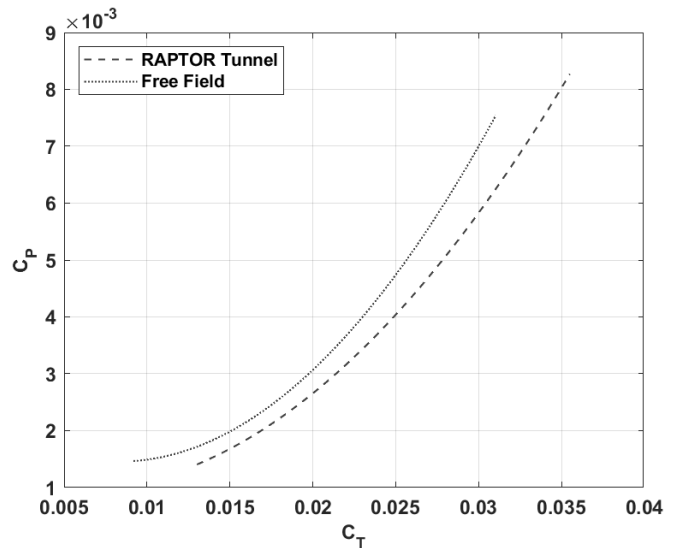
Figure 33. Predicted torque coefficient vs. thrust coeffi-cient for a single 4-bladed MSH rotor at RPM=1900, for-ward speed=10 m/s, and pitch angle =0 deg in free field and in the RAPTOR tunnel.

Figure 34. Predicted C_T vs. collective for a single 4-bladed MSH rotor in RAPTOR tunnel at RPM=2100.

Figure 35. Predicted C_P vs. collective for a single 4-bladed MSH rotor in RAPTOR tunnel at RPM=2100.

Figure 36. Predicted drag coefficient vs. collective for a single 4-bladed MSH rotor in RAPTOR tunnel at RPM=2100.

CONCLUDING REMARKS

Much like the thoroughly tested NACA airfoil series that is often used as generic references for Earth-bound wings, Mars Aerodynamic Rotor Test-I seeks to establish a preliminary methodology for characterizing aerodynamic loads of airfoils tailored to fly in Mars conditions—starting with a generic reference blade now being used in association with the MSH. Using basic conditions and assumptions to first predict rotor loadings via CHARM simulations to size the physical test stands, the data from planned experiments can be used to help validate and improve the simulation results. Iteratively using simulations and wind tunnel testing to gather new insight on the aerodynamics of Martian rotorcrafts is one of the next steps for establishing a library of well-documented airfoils suitable for flight on the Red Planet.

The current CHARM results serve as a guide for developing test matrices and identifying potential risky conditions such as high collective or tunnel speeds to avoid rotor stall, or high rotor loads that can damage the rotor blade, test stand, equipment, and facility. The current results suggest trimming the 4-bladed MSH rotor to C_T/σ below 0.13 while staying at an RPM<2100 would be prudent. Also, the results suggest avoiding exceeding 12 degree collective to prevent possible high rotor blade loads. In addition, changing tunnel speeds should be performed at collective=0 degree.

After the 2-bladed rotor spin up test (SUT) is completed, the data can be used to inform the forward flight results. Also, the as-built rotor blades need to be laser-scanned to validate the rotor geometry used for the simulations in this paper.

In addition, generating a set of airfoil tables for PAL conditions is recommended for further computational study associated with correlating performance predictions with their wind tunnel experimental counterpart results.

While rotorcraft flight on Mars has been proven feasible, and the future of Martian rotorcrafts is indeed bright, there is a significant amount of work required here on Earth as we seek to improve the next generation of Mars helicopters

Author contact

Dorsa Shirazi	dorsa.shirazi@nasa.gov
Athena Chan	athena.chan@nasa.gov
Wayne Johnson	wayne.johnson@nasa.gov

APPENDIX A

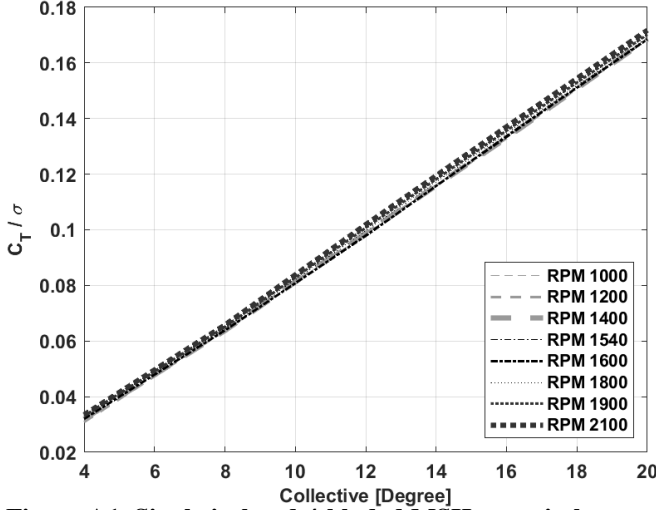The additional simulation results for MSH rotor in hover:

Figure A1. Single isolated 4-bladed MSH rotor in hover – C_T/σ vs collective.
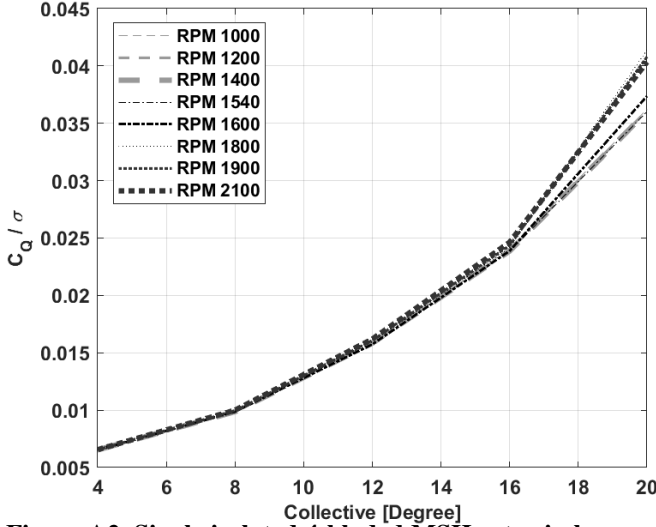

Figure A2. Single isolated 4-bladed MSH rotor in hover – C_Q/σ vs collective.
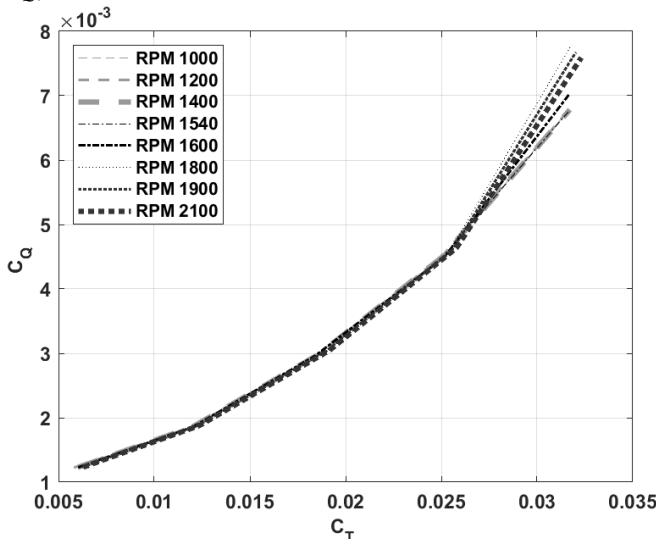

Figure A3. Single isolated 4-bladed MSH rotor in hover – C_Q vs C_T.

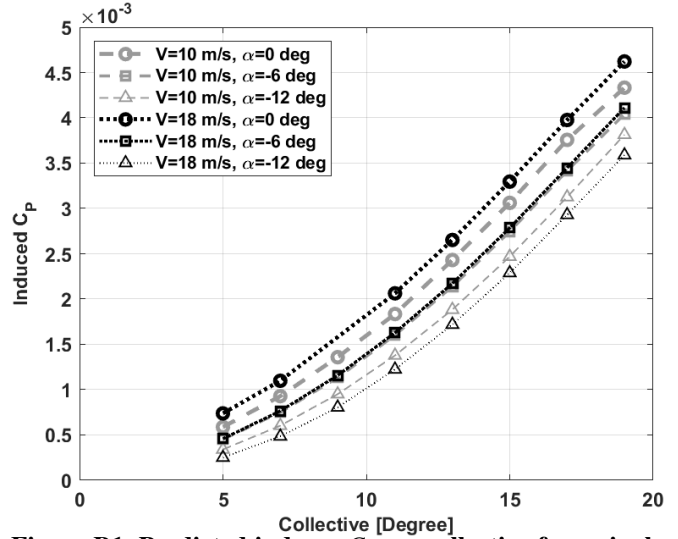# APPENDIX B

The additional simulation results:

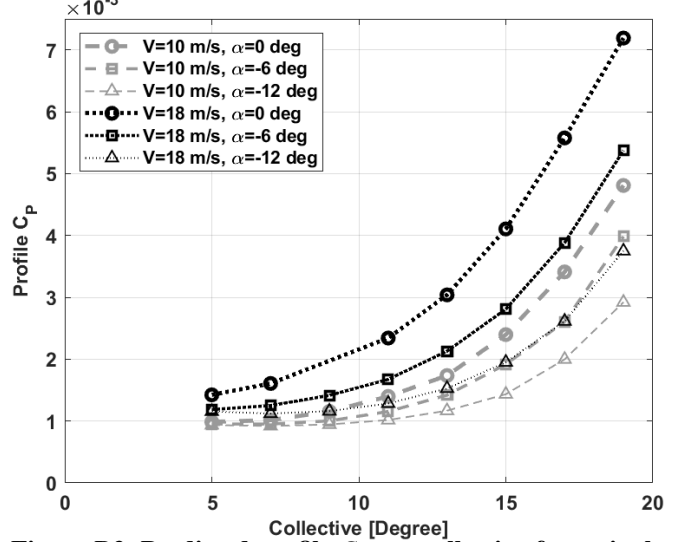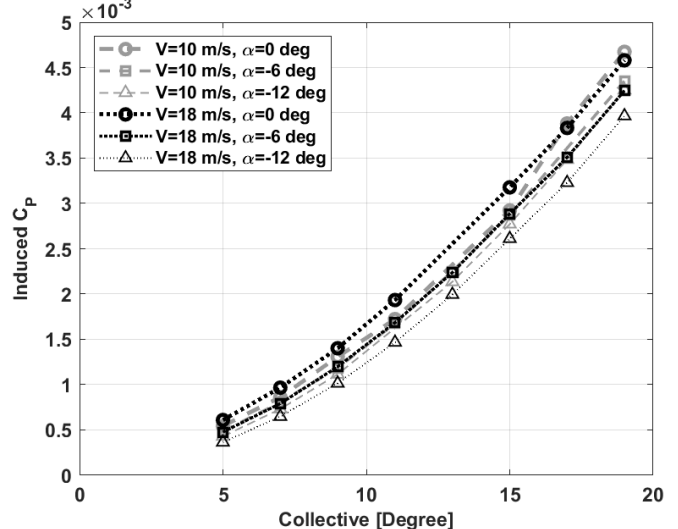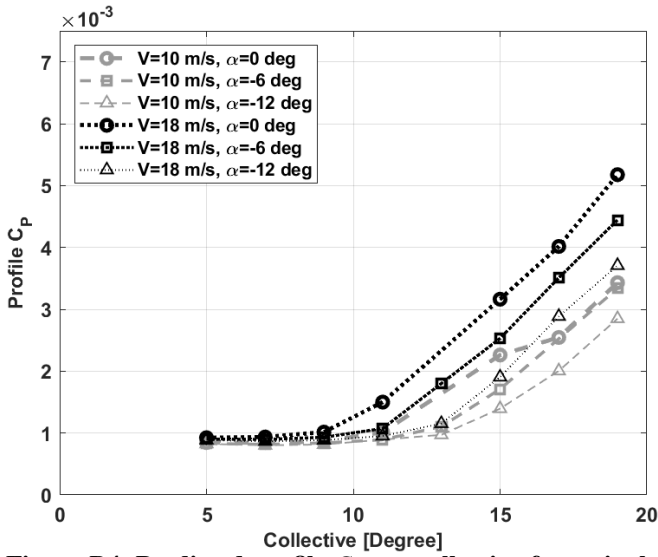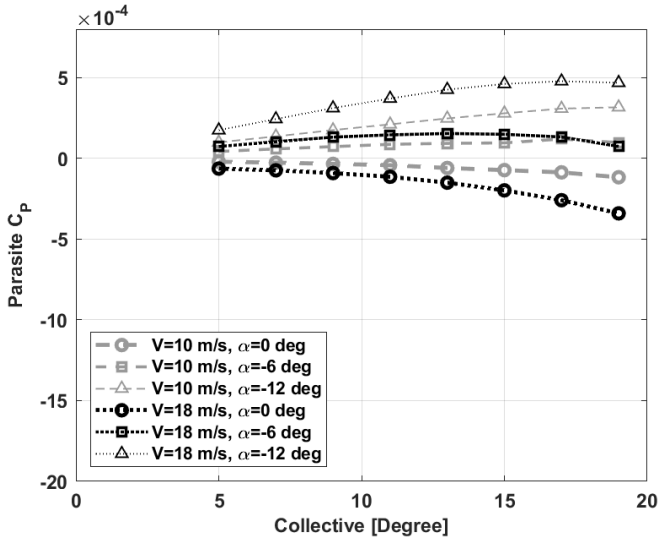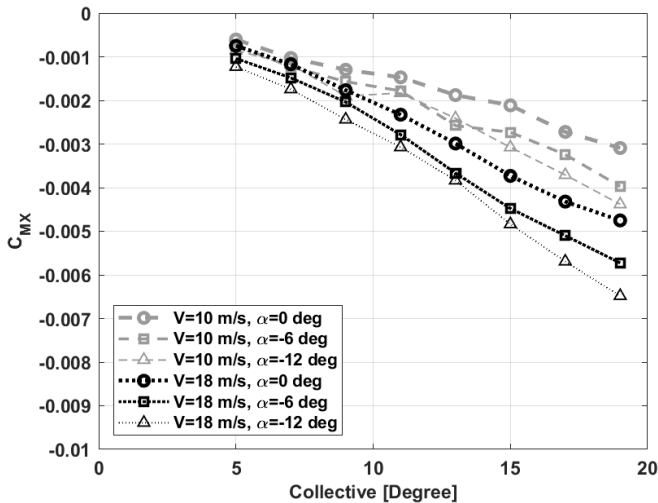**Figure B1.** Predicted induces C_P vs. collective for a single 4-bladed MSH rotor in RAPTOR tunnel - RPM=1000.

Figure B2. Predicted profile C_P vs. collective for a single 4-bladed MSH rotor in RAPTOR tunnel at RPM=1000.

Figure B3. Predicted induces C_P vs. collective for a single 4-bladed MSH rotor in RAPTOR tunnel at RPM=1900.

Figure B4. Predicted profile C_P vs. collective for a single 4-bladed MSH rotor in RAPTOR tunnel at RPM=1900

Figure B7. Predicted C_{M_Y} vs. collective for a single 4-bladed MSH rotor in RAPTOR tunnel at RPM=2100.
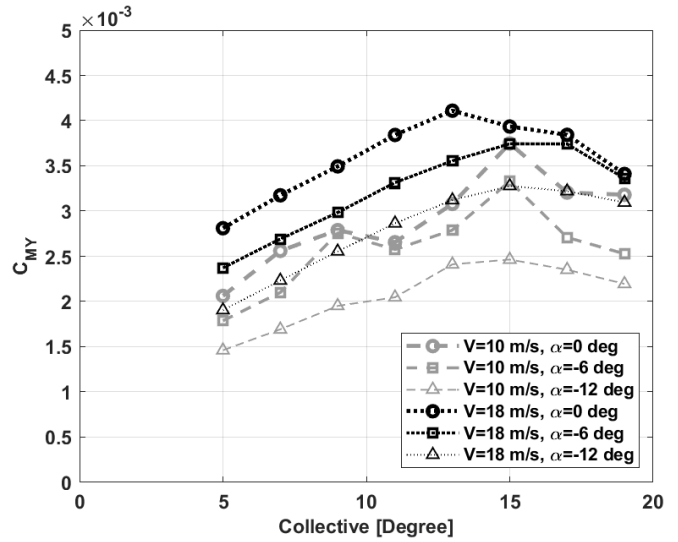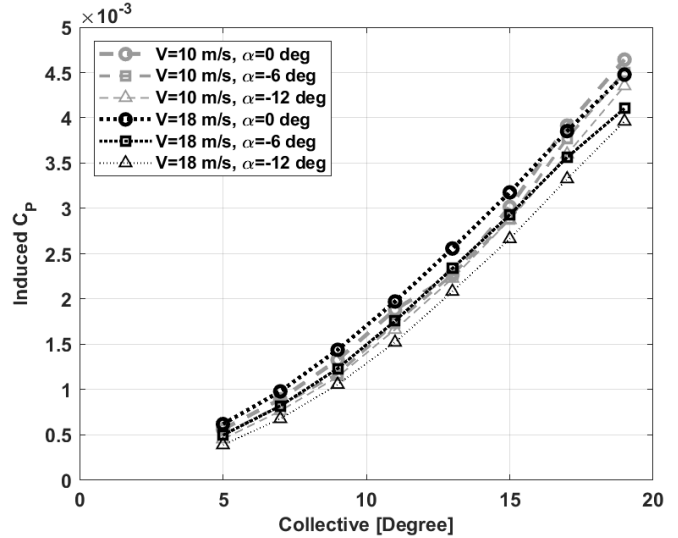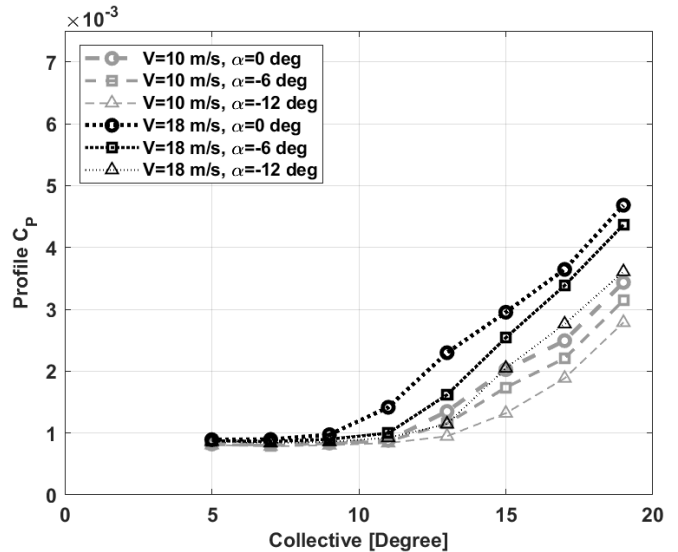

Figure B5. Predicted parasite C_P vs. collective for a single 4-bladed MSH rotor in RAPTOR tunnel at RPM=2100.

Figure B8. Predicted induces C_P vs. collective for a single 4-bladed MSH rotor in RAPTOR tunnel at RPM=2100.

Figure B6. Predicted C_{M_X} vs. collective for a single 4-bladed MSH rotor in RAPTOR tunnel at RPM=2100.

Figure B9. Predicted profile C_P vs. collective for a single 4-bladed MSH rotor in RAPTOR tunnel at RPM=2100.

15

APPENDIX C

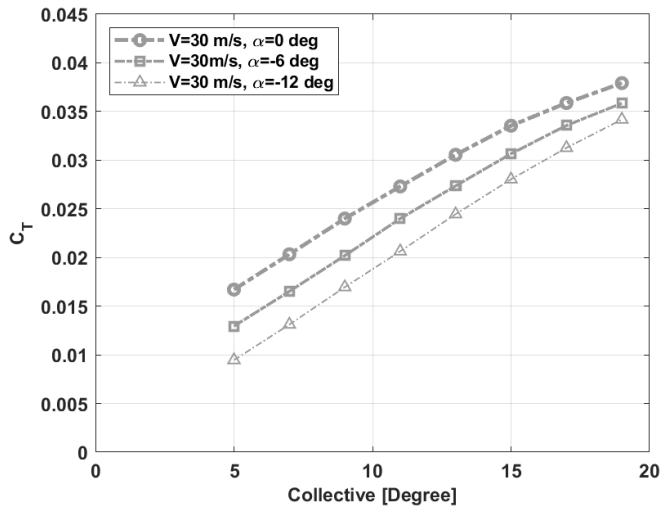The additional simulation results for tunnel speed of 30 m/s.

Figure C1. Predicted profile C_T vs. collective for a single 4-bladed MSH rotor in RAPTOR tunnel at RPM=1900.
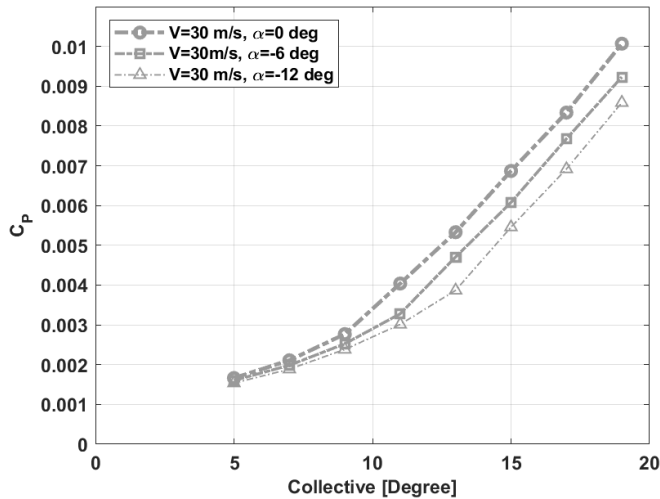

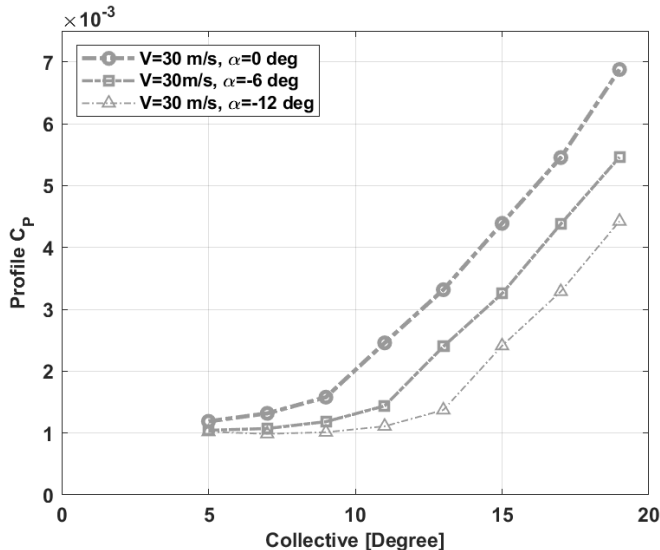**Figure C2. Predicted C_P vs. collective for a single 4-bladed MSH rotor in RAPTOR tunnel at RPM=1900.**

Figure C3. Predicted profile C_P vs. collective for a single 4-bladed MSH rotor in RAPTOR tunnel at RPM=1900.
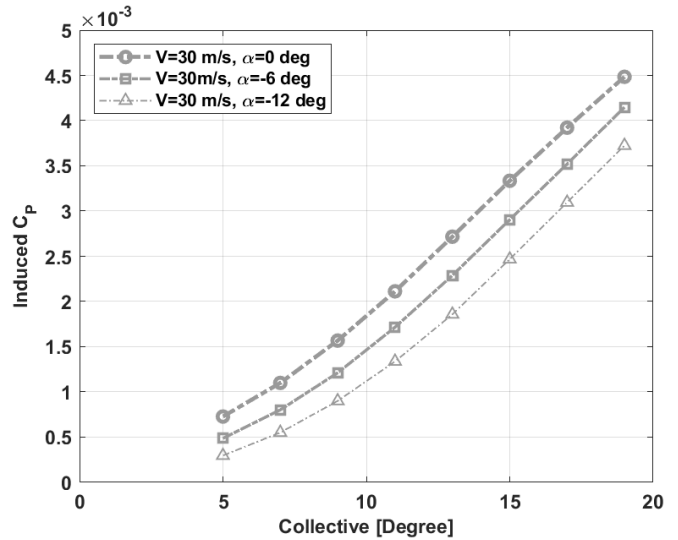

Figure C4. Predicted C_T vs. collective for a single 4-bladed MSH rotor in RAPTOR tunnel at RPM=1900.
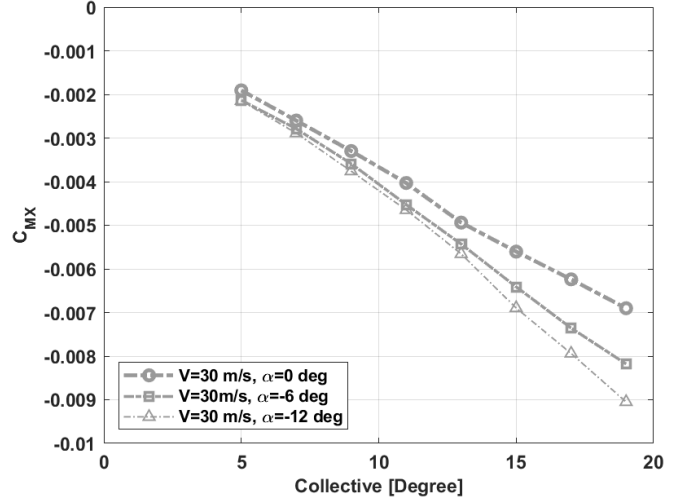

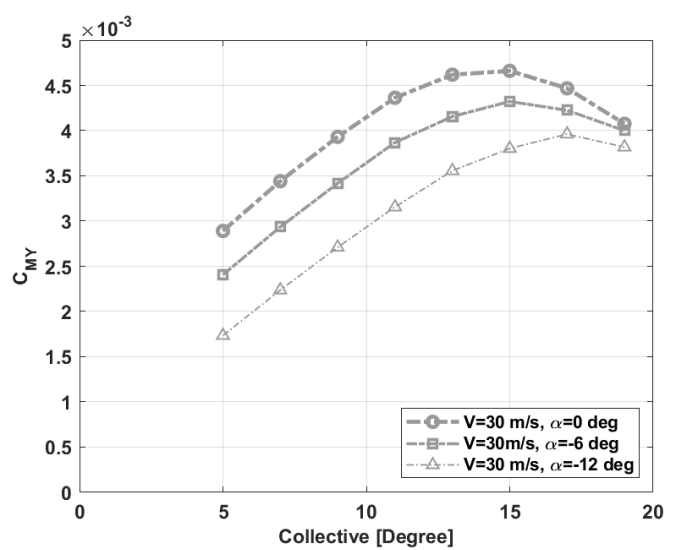**Figure C5. Predicted C_{M_X} vs. collective for a single 4-bladed MSH rotor in RAPTOR tunnel at RPM=1900.**

Figure C6. Predicted C_{M_Y} vs. collective for a single 4-bladed MSH rotor in RAPTOR tunnel at RPM=1900.

16

REFERENCES

1. Grip, H., Johnson, W., Malpica, C., Scharf, D., Mandic, M., Young, L., Allany, B., Mettlerz, B., and San Martin, M., "Flight Dynamics of a Mars Helicopter," 43rd European Rotorcraft Forum, Milan, Italy, September 2017.

2. Young, L., Chen, R., Aiken, E., and Briggs, G., "Design Opportunities and Challenges in the Development of Vertical Lift Planetary Aerial Vehicles," American Helicopter Society International Vertical Lift Aircraft Design Conference, San Francisco, CA, January 2000.

3. Johnson, W., Withrow-Maser, S., Young, L., Malpica, C., Koning, W., Kuang, W., Fehler, M., Tuano, A., Chan, A., A.and Datta, Chi, C., Lumba, R., Escobar, D., Balaram, J., Tzanetos, T., and Grip, H., "Mars Science Helicopter Conceptual Design," NASA/TM- 220485, 2020.

4. Wachspress, D., Quackenbush, T., and Boschitsch, A., "Rotorcraft Interactional Aerodynamics with Fast 13 Vortex/Fast Panel Methods," *Journal of the American Helicopter Society*, Volume 48, Number 4,, October 2003.

5. Wachspress, D., Quackenbush, T., and Boschitsch, A., "First-Principles Free-Vortex Wake Analysis for Helicopters and Tiltrotors," American Helicopter Society 59th Annual Forum, Phoenix, AZ, May 2003.

6. Cummings, H., "Planetary Aeolian Laboratory at NASA Ames Research Center," science.nasa.gov, *https : //science.nasa.gov/wp − content/uploads/2023/06/PAL_Updated.pdf*, June, 2023.

7. Ament, G., and Koning, W., "Isolated Rotor Forward Flight Testing from One Atmosphere Down to Martian Atmospheric Densities," AHS Technical Meeting on Aeromechanics Design for Vertical Lift, Holiday Inn at Fisherman's Wharf, San Francisco, CA, January 2018.

8. Harding, J., Moody, S., Mansur, M., and Tischler, M., "Development of Modern Control Laws for the AH-64D in Hover - Low Speed Flight," American Helicopter Society 62nd Annual Forum, Phoenix, AZ, May 2006.

9. Christensen, K., K., C., Griffith, C., Ivler, C., Tischler, M., and Harding, J., "Flight Control Development for the ARH-70 Armed Reconnaissance Helicopter Program," American Helicopter Society 63rd Annual Forum, Virginia Beach, VA, May 2007.

10. Johnson, W., "CAMRAD II Comprehensive Analytical Model of Rotorcraft Aerodynamics and Dynamics," Johnson Aeronautics, Palo Alto, CA, 2005.

11. Young, L., and et al, "Experimental Investigation and Demonstration of Rotary-Wing Technologies for Flight in the Atmosphere of Mars," the 58th Annual Forum of the AHS, International, Montreal, Canada, June 2002.

12. Quackenbush, T., and Bliss, D., "Free Wake Calculation of Rotor Flow Fields for Interactional Aerodynamics," American Helicopter Society 44th Annual Forum, Washington DC, June 1988.

13. Shirazi, D., "Comparison of the CHARM Predictions of the Multirotor Test Bed with Wind Tunnel Experimental Results," VFS Aeromechanics for Advanced Vertical Flight Technical Meeting, San Jose, CA, January 2022.

14. Dull, C., Wagner, L., Young, L., and Johnson, W., "Hover and Forward Flight Performance Modeling of the Ingenuity Mars Helicopter," VFS Aeromechanics for Advanced Vertical Flight Technical Meeting, San Jose, CA, January 2022.

15. Koning, W., Romander, E., and Johnson, W., "Optimization of Low Reynolds Number Airfoils for Martian Rotor Applications Using an Evolutionary Algorithm," 6.2020-0084, AIAA Science and Technology Forum and Exposition (AIAA SciTech), Orlando, FL, January 2020.

16. Koning, W., Romander, E., Cummings, H., Perez Perez, N., and Buning, P., "On Improved Understanding of Airfoil Performance Evaluation Methods at Low Reynolds Numbers," *Journal of Aircraft*, Volume 60, No. 2, March 2023.